



OPEN ACCESS

Low-Cost and Fast-Response Resistive Humidity Sensor Comprising Biopolymer-Derived Carbon Thin Film and Carbon Microelectrodes

To cite this article: Shalik Ram Joshi *et al* 2020 *J. Electrochem. Soc.* **167** 147511

View the [article online](#) for updates and enhancements.

 The Electrochemical Society Advancing solid state & electrochemical science & technology 2021 Virtual Education Fundamentals of Electrochemistry: Basic Theory and Kinetic Methods Instructed by: Dr. James Noël Sun, Sept 19 & Mon, Sept 20 at 12h–15h ET Register early and save!	
---	--



Low-Cost and Fast-Response Resistive Humidity Sensor Comprising Biopolymer-Derived Carbon Thin Film and Carbon Microelectrodes

Shalik Ram Joshi,^{1,=} Beomsang Kim,^{1,=} Shin-Kwan Kim,¹ Wonho Song,² Kibog Park,^{2,3} Gun-Ho Kim,^{1,z} and Heungjoo Shin^{1,z} 

¹Department of Mechanical Engineering, Ulsan National Institute of Science and Technology (UNIST), Ulsan, Republic of Korea

²Department of Physics, Ulsan National Institute of Science and Technology (UNIST), Ulsan, Republic of Korea

³Department of Electrical Engineering, Ulsan National Institute of Science and Technology (UNIST), Ulsan, Republic of Korea

In this study, we present a highly responsive room-temperature resistive humidity sensor based on a shellac-derived carbon (SDC) active film deposited on sub-micrometer-sized carbon interdigitated electrodes (cIDEs). This monolithic carbon-based sensor demonstrates an excellent linear relationship with humidity and ohmic contact between the active carbon film and carbon electrodes, which results in low noise and low power consumption (~ 1 mW). The active SDC film is synthesized by a single-step thermal process, wherein the temperature is found to control the amount of oxygen functional moieties of the SDC film, thereby providing an efficient means to optimize the sensor response time, recovery time, and sensitivity. This SDC-cIDEs-based humidity sensor exhibits an excellent dynamic range (0%–90% RH), a large dynamic response (50%), and high sensitivity (0.54%/RH). In addition, the two-dimensional feature (thickness ~ 10 nm) of the SDC film enables a swift absorption/desorption equilibrium, leading to fast response (~ 0.14 s) and recovery (~ 1.7 s) under a humidity range of 0%–70% RH. Furthermore, the thin SDC-based sensor exhibited excellent selectivity to humidity from various gases, which in combination with its fast response/recovery promises its application for an instant calibration tool for gas sensors.

© 2020 The Author(s). Published on behalf of The Electrochemical Society by IOP Publishing Limited. This is an open access article distributed under the terms of the Creative Commons Attribution 4.0 License (CC BY, <http://creativecommons.org/licenses/by/4.0/>), which permits unrestricted reuse of the work in any medium, provided the original work is properly cited. [DOI: 10.1149/1945-7111/abc592]



Manuscript submitted September 18, 2020; revised manuscript received October 20, 2020. Published November 6, 2020. *This paper is part of the JES Focus Issue on IMCS 2020.*

Supplementary material for this article is available [online](#)

Humidity monitoring is important in various applications including electronics, agriculture, environmental monitoring, and biomedical analysis.¹ Furthermore, the advancement in internet of things (IoT) applications necessitate the essential characteristics for humidity sensors such as low power consumption, room-temperature operation, small size, and compatibility with other sensor platforms (e.g., thermal and chemical compatibility in fabrication, excellent selectivity from other species for sensor calibration),^{2–6} in addition to the conventional requirements such as high sensitivity, fast response, long-term stability, and cost effectiveness. Particularly, the gas sensors used for air-quality monitoring and breath-based diagnostics are largely affected by humidity and therefore require humidity calibration, which requires both rapid response time and high selectivity for instant and accurate calibration.^{7,8}

Various metal oxides (MOx) and their composites have been extensively investigated as sensing materials, owing to their low cost, high surface-to-volume ratio, fast kinetics, high sensitivity, high sensor response, and compatibility with modern integrated circuit technology.^{9–12} However, MOx based humidity sensors require the integration of high-power heaters for high sensitivity and fast response, which not only leads to a complicated and expensive fabrication process, but also limits their application in battery-driven IoT devices.^{8,13,14} Moreover, their high-temperature operation causes undesirable long-term drift problems owing to the sintering effects at the grain boundaries, resulting in the degradation of the selectivity and long-term stability.¹⁴

The potential of graphene oxide (GO), which has a large surface area and oxygen moieties, as an active humidity sensing material has been previously demonstrated.^{15,16} Specifically, GO-based humidity sensors have recently exhibited their capability of room-temperature operation,¹⁷ which eliminates the necessity for high power consumption heaters.

However, despite these advantages, the practical applicability of the GO-based humidity sensors is restricted by poor reliability under high humidity conditions; this is due to the excessive water absorption between the GO layers as well as the poor adhesion of the GO active film to the substrate or electrical leads.^{15,18} In contrast, reduced graphene oxide (rGO) is electrically more conductive and provides stable sensing, but it persists with disadvantages such as limited humidity response¹⁹ and poor reliability due to its poor adhesion.¹⁵ Moreover, GO-based sensors have demonstrated their sensitivity to other gas environments such as NO₂, H₂, and NH₃, which limits their selective humidity monitoring and applicability as a calibration tool.^{19,20}

Here, we present a novel monolithic carbon-based resistive humidity sensor using a biopolymer-derived thin carbon film coated on carbon interdigitated electrodes (cIDEs), which is capable of room-temperature operation, and exhibits excellent sensitivity, selectivity, and long-term reliability. A variety of biomaterials have been actively studied for the simple and cost-effective fabrication of thin carbon films for various sensor applications.^{21–23} Here, in this report, the carbon film which functions as an active humidity sensing material was synthesized from low-cost biopolymer, namely shellac which has long-chain aliphatic carbon atoms with low bond dissociation energy that allows the formation of highly sp² hybridized carbon networks at relatively lower annealing temperatures than the other synthetic polymers.^{24,25} The active film is directly synthesized on a substrate by a single-step thermal process, which promotes adhesion between the active film and substrate, thereby enhancing the sensor reliability and long-term stability. Furthermore, the amount of oxygen-containing functional groups—and therefore, the sensor characteristics—were observed to vary sensitively with the process temperature, as confirmed by X-ray photoelectron spectroscopy (XPS) and Raman spectroscopy. Relative humidity (RH) was detected by measuring the electrical resistance of the thin Shellac derived carbon (SDC) film with sub-micrometer-sized cIDEs, which were fabricated using carbon microelectromechanical systems (C-MEMS). This process enables a simple wafer-level fabrication of micro/nanometer-sized three-dimensional

⁼These authors contributed equally to this work.

^zE-mail: gunhokim@unist.ac.kr; hjshin@unist.ac.kr

(3D) carbon structures by the pyrolysis of prepatterned polymer structures. ^{26–31} Unlike the carbon thin film-based devices with metal electrodes, ^{32,33} the cIDEs with small gaps did not exhibit noticeable contact resistance or Schottky barrier with SDC film; therefore, high signal-to-noise ratio, low power consumption, and superior reliability could be obtained. Moreover, the fabrication processes of the SDC and cIDEs are chemically and thermally compatible, thereby facilitating a cost-effective wafer-level fabrication of humidity sensors. To investigate the humidity sensing characteristics of the thin SDC film, impedance as well as DC responses to humidity were measured. The Nyquist plots exhibited a semicircular like behavior without displaying Warburg behavior, indicating the dominance of electronic conduction in SDC thin film-based humidity sensor. The resultant monolithic carbon resistive humidity sensor exhibited fast response, fast recovery, high sensitivity, and excellent reliability under a wide humidity range. Furthermore, the present sensor also exhibited excellent selectivity to humidity from various gaseous molecules, and therefore has potential applications as a prompt calibration tool for gas sensors with characteristics that significantly vary with humidity.

Experimental

Materials.—Shellac flakes were purchased from Shellac Shack, USA. Isopropanol (IPA) (99.5%) was purchased from Sigma-Aldrich (USA). Two types of negative photoresists (SU-8 2002 and 2025) were purchased from MicroChem. Corp. (USA).

Fabrication of carbon IDEs.—Figures 1a–1c shows the fabrication of sub-micrometer-sized carbon IDEs by the pyrolysis of prepatterned photoresist structures: A thin layer of negative photoresist (SU-8 2002, 2 μm) was spin coated on a 6 inch silicon wafer, which was insulated with a 1 μm thick thermally grown SiO₂ layer. The photoresist layer was UV-exposed via a photomask using a mask aligner (MA/BA6-8, SÜSS MicroTec SE, Germany) and the exposed photoresist was developed using the SU-8 Developer, forming IDE-shaped polymer structures, as shown in Fig. 1a. Then, as shown in Fig. 1b, thick photoresist pad structures (SU-8 2025, 25 μm) were patterned on the prepatterned IDE-shaped polymer structures to form thick carbon pads for reducing the electrical resistance between the cIDEs and source meter. The patterned photoresist structures were converted into monolithic hierarchical carbon electrodes (thin cIDE fingers and thick planar carbon electrodes, as shown in Fig. 1c) under vacuum by a two-step thermal process, including vacuum pyrolysis and rapid thermal annealing (RTA); the following is a description of the two steps: Firstly, the polymer structures were pyrolyzed in a vacuum furnace (DMTF15/145-400, Daemyoung Enterprise Co., Ltd., Korea). The temperature of the furnace was increased and maintained for 1 h at 350 °C to alleviate the effect of the rapid volume reduction. ³⁴ Then, the furnace was further heated to 700 °C and held at this temperature for 1 h. The pyrolyzed carbon structures were naturally cooled to minimize the thermal stress on the sample. Secondly, the carbon sample was annealed at 1000 °C for 1 min using an RTA system (KVR-6000, Korea Vacuum Tech. Ltd., Korea) to enhance the electrical conductivity of the carbon electrodes. ³⁵

Synthesis of SDC film onto carbon electrodes.—Shellac flakes (4 g) were dissolved in 100 ml IPA while stirring at 60 °C for 1 h. The obtained solution was uniformly coated on the carbon IDEs using a manual spray coater (Fig. 1d). These spray-coated samples were dried at 25 °C for 30 min and subsequently annealed at various temperatures (550 °C–700 °C) under low vacuum conditions (0.16 mbar), at a ramping rate of 3 °C min⁻¹ for 30 min (Fig. 1e). In this study, the samples have been labeled as SDC-xxx, where xxx is the annealing temperature.

Patterning of SDC film on carbon IDEs.—The SDC film was locally defined at the cIDEs, as shown in Figs. 1f–1h. Thus, the electrical current path was limited to the SDC film between the facing electrodes of the IDE fingers, thereby eliminating the effect of

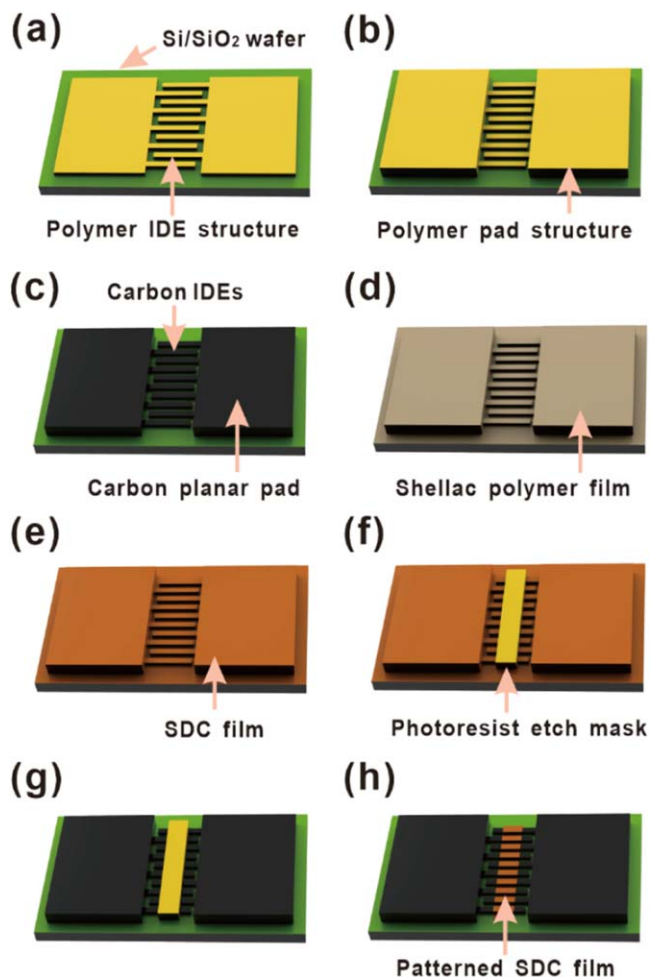


Figure 1. Schematic of the fabrication steps of the SDC film based humidity sensor: (a) photolithography for polymer IDE structures using a thin photoresist layer; (b) photolithography for polymer pad structures using a thick photoresist layer; (c) pyrolysis for sub-micrometer-scale cIDEs and thick planar pads; (d) spray coating of the shellac solution on the substrate; (e) annealing the shellac solution to synthesize the SDC film; (f) photolithography for an etch mask; (g) selective SDC film removal using oxygen plasma; (h) photoresist removal.

the electric field between the IDEs and the thick carbon planar electrodes on the humidity sensor signal. The patterning was performed after synthesizing the SDC film on the cIDEs. A photoresist (NR9-8000, Futurrex Inc., USA) etching mask was patterned on the SDC film-coated carbon IDEs by photolithography. Subsequently, the exposed SDC film was subjected to selective oxygen plasma etching (PR Asher, KAMI, Germany), after which, the patterned polymer was removed using a photoresist remover solution and the sample was rinsed with deionized water.

Characterization.—The microstructure analysis of the obtained products was carried out using a scanning electron microscope (SEM) (Quanta 200 FEG, FEI, USA). The Raman spectra of the samples were collected in a backscattering mode using ultra-high-throughput spectrometers (Al-pha300R, WITec, Germany). The XPS measurements were performed using Thermo Scientific K-Alpha XPS system (Thermo Fisher Scientific, UK) equipped with a double-focusing hemispherical analyzer and monochromatic Al K_α source (1486.6 eV). The *I*-*V* characteristics of the humidity sensors were measured using a Keithley-2450 Source Meter (Keithley Instruments Inc., USA) to confirm the ohmic contact between the cIDEs and SDC film. The film thickness was measured by atomic force microscopy (AFM) (Multimode V, Bruker, USA). The nature

of the charge carriers of the SDC films was investigated by measuring the Hall effect using Hall bar patterned SDC films. The Hall measurement setup was calibrated using commercially available *p*-type and *n*-type silicon wafers before measuring the Hall effect of the SDC thin film. The impedance behavior of the SDC film-based humidity sensor for various % RH was characterized using a potentiostat (Ivium Stat, Ivium Technologies, Netherlands; 1 V, 100 Hz–1 MHz). To characterize the response time of the SDC film based humidity sensors, we set up a customized humidity/temperature-controlling system enabling the instantaneous exchange of the chamber humidity conditions ranging from highly humid (70% RH) to dry air (0% RH). The customized test system comprised solenoid valves (S10MM20-24-2, Pneumadyne Inc., USA), a humidity/temperature sensor (SHT15, Sensirion), a microcontroller board (Arduino Uno, Arduino cc), and a microscope incubator (CU-501, Live Cell Instrument). The solenoid valve motion was programmed using the LabVIEW software (National Instruments). A gas sensitivity test was performed for various gases (NO_2 , H_2 , and CH_4) under atmospheric pressure. The gas concentration was controlled by mixing the target gas with air using mass flow controllers (GMC1200, ATOVAC, Korea). The resistance of the humidity sensor was measured using the abovementioned source meter.

Results and Discussion

Morphology of the humidity sensor based on the biopolymer-derived carbon film.—Figure 2 shows the SEM images of the thin carbon film based humidity sensors prepared by integrating SDC films on sub-micrometer-sized cIDEs. Because of a significant volume reduction during pyrolysis ($\sim 90\%$), the microscale photoresist IDE structures (width = $1\ \mu\text{m}$, height = $2\ \mu\text{m}$) were shrunk to sub-micrometer-sized carbon IDEs (width = $600\ \text{nm}$, height = $300\ \text{nm}$, electrode gap = $1.5\ \mu\text{m}$). Owing to the small electrode size, the total electrode length of the facing electrodes could be extended up to $100\ \text{mm}$ for a $100\ \mu\text{m} \times 2\ \text{mm}$ sensing area of the SDC film. This reduced the electrical resistance of the film situated between the facing fingers of the IDEs, enabling effective electrical resistance measurement even for films with relatively low electrical conductivity. After the synthesis of the SDC film on the carbon IDEs, it was further patterned by successive photolithography and oxygen plasma etching, as shown in Figs. 1f–1h, which provided a definite sensing area and thereby, a means to precisely characterize the SDC film based humidity sensor.

The surface morphology of the SDC film was analyzed using SEM and AFM. The SDC film was uniformly deposited without the formation of any noticeable grain boundaries or cracks, even at a large scale, as shown in Fig. S1 (available online at [stacks.iop.org/JES/](https://stacks.iop.org/JES/167/147511/mmedia)

[167/147511/mmedia](https://stacks.iop.org/JES/167/147511/mmedia)). Moreover, the conformal quality of the SDC film was observed even in the small gaps between the repeated 3D carbon fingers, as shown in Figs. 2a–2c. To measure the thickness of the thin SDC film using AFM, the SDC films were patterned into small squares using the same processes that were used for the carbon film coating on the cIDEs (Figs. 1f–1h). The carbon films exhibited an average thickness of $\sim 10\ \text{nm}$, as shown in Fig. S2, which confirmed its 2D nature. Furthermore, the AFM data indicated a fairly smooth surface with a roughness (R_a) of $\sim 0.25\ \text{nm}$, which is close to the roughness of the SiO_2 -insulated Si substrate. Notably, the SDC film exhibited similar thickness regardless of the annealing temperature; the reason for this can be inferred from the thermogravimetric analysis (TGA) results of the shellac polymer samples (Fig. S3): The weight loss of shellac can be ascribed to the dehydration and dehydrogenation process, at low ($<150\ ^\circ\text{C}$) and intermediate ($<450\ ^\circ\text{C}$) temperatures, respectively. At $550\ ^\circ\text{C}$, the biopolymer precursor was not fully carbonized and its weight continued to decrease (76 wt% loss), as evidenced by its TGA curve (Fig. S3), Raman spectra (Fig. S4a), and high-resolution C-1s XPS spectra (Fig. S4b). However, no further significant weight loss of the biopolymer precursor was observed from $600\ ^\circ\text{C}$ onwards. Thus, most of the weight loss occurred between $400\ ^\circ\text{C}$ and $600\ ^\circ\text{C}$, after which there was a negligible weight change. Therefore, the SDC films treated at temperature higher than $600\ ^\circ\text{C}$ exhibited similar film thickness.

Microstructure and composition of the biopolymer-derived carbon film.—As shown in Figs. 3a and 3c, the high-resolution C-1s XPS spectra show the evolution of the oxygen-containing functional groups with increasing annealing temperature. The XPS spectra were deconvoluted into four peaks of different carbon environments: (C=C) at $284.2\ \text{eV}$, (C–OH) at $285.3\ \text{eV}$, (C=O) at $288.1\ \text{eV}$, and a satellite peak at $291\ \text{eV}$ due to π – π interactions. Compared to the XPS data for the SDC-550 sample (Fig. S4b), the development of a new peak at $284.2\ \text{eV}$ confirms the initiation of the graphitization at $600\ ^\circ\text{C}$. As the annealing temperature increased from $600\ ^\circ\text{C}$ to $700\ ^\circ\text{C}$, the sp^2 hybridized carbon network significantly increased from $\sim 55\%$ to 80% and the content of the oxygen-containing functional groups was reduced (Fig. 3c). The Raman spectra of the samples (Fig. 3b) exhibited two prominent features, namely the D and G bands, which are attributed to the sp^3 defect sites and the sp^2 carbon atoms with in-plane vibrations, respectively.³⁶ The G band displayed a systematic redshift with the annealing temperature, which indicates an increase in the sp^2 hybridized carbon network (Fig. 3d). Furthermore, as shown in Fig. 3d, the D/G intensity ratio (I_D/I_G) also decreases from 0.88 (SDC-600) to 0.63 (SDC-700), indicating relatively fewer defects and structural disorder in SDC-700.

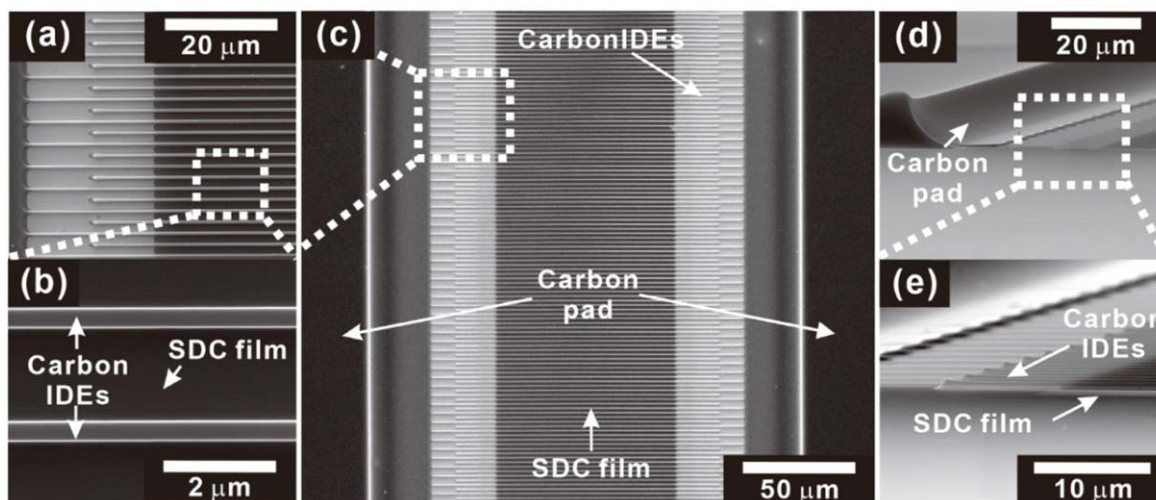


Figure 2. SEM images of the SDC film based humidity sensor: (a)–(c) top view, (d), (e) bird's eye view.

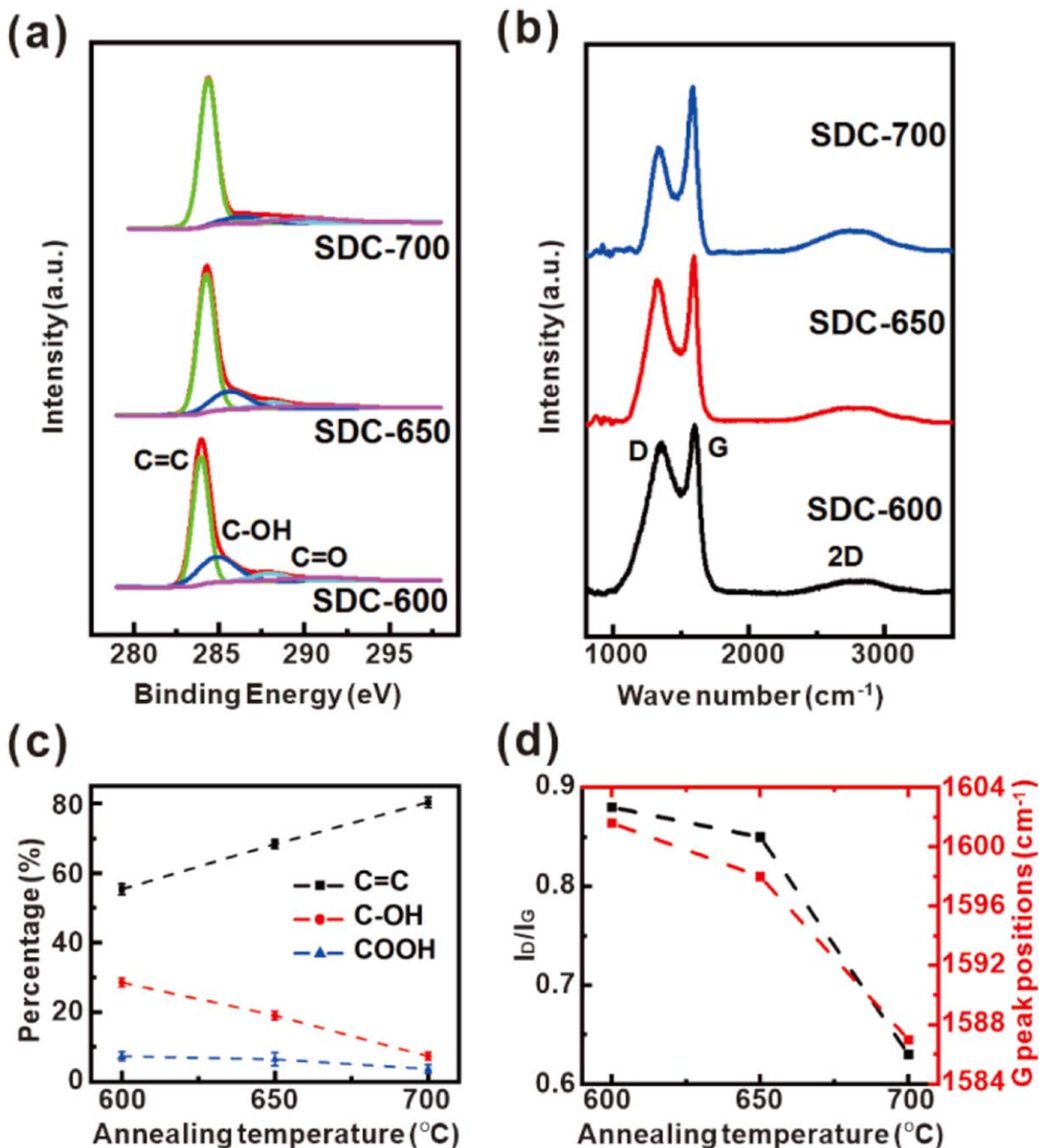


Figure 3. XPS and Raman spectra of the SDC films annealed at various temperatures (600 °C, 650 °C, and 700 °C): (a) high-resolution C-1s XPS spectra (red curve: cumulative peak fitting, green curve: C=C, blue curve: C-OH, cyan curve: C=O, and magenta curve: $\pi-\pi$ interactions); (b) Raman spectra; (c) weight percentage of various oxygen-containing functional groups (black square: C=C, red circle: C-OH, blue triangle: COOH) calculated from the XPS data; (d) I_D/I_G intensity and G peak position depending on the SDC annealing temperature.

Humidity sensing test.—The electrical properties of the SDC films were characterized by measuring the I - V curve, as shown in Fig. S5. The SDC films integrated on the cIDEs exhibited an excellent ohmic behavior, confirming the excellent electrical and thermal compatibility between the SDC film and the pyrolyzed cIDEs. In the present sensor electrode configuration, the cIDE fingers were connected to the thick and wide carbon pads (Figs. 2c and 2d, width = 2 mm, thickness = 6 μm) to reduce the effect of the electrode resistance on the SDC film resistance measurement. This also ensured the excellent ohmic behavior of the SDC films. Besides, the film resistance decreases linearly as the gap between the carbon electrodes decreases, as shown in Fig. S6, which confirms the uniform coating of the SDC film on the 3D carbon electrodes separated by a small gap. As shown in Fig. S5, the

resistance of SDC-550 is significantly higher than the SDC films annealed at higher temperatures, suggesting that SDC-550 is not fully carbonized and contains a large number of defects; this is also confirmed by the TGA, XPS, and Raman spectra (Figs. S3 and S4). Thus, based on TGA and electrical measurements, the SDC-550 sample was not considered for the humidity sensing test.

The sensing properties of the present SDC film based humidity sensors were evaluated by measuring the electrical resistance of the humidity sensor in a constant humidity and temperature chamber (TH-ME-065, JEIO Tech., Korea), under varying humidity conditions (0%–90% RH) in air at a constant temperature (25 °C). In this study, humidity sensor response has been defined as the percentage of resistance change in the sensor relative to the resistance measured under dry conditions (0% RH):

$$\text{Response}(\%) = \left| \frac{\Delta R}{R} \right| \times 100 = \left| \frac{R_h - R}{R} \right| \times 100 \quad [1]$$

where R is the resistance of the sensor in the presence of dry air (0% RH), and R_h is the resistance in the presence of humid air at a given RH value. Based on this, the sensitivity (S) of the sensor can be defined as:

$$S = \frac{1}{\Delta RH} \left(\left| \frac{\Delta R}{R} \right|_{\max} - \left| \frac{\Delta R}{R} \right|_{\min} \right) \quad [2]$$

where ΔRH is the range of RH in the humidity test.

The resistive responses under various humidity conditions measured using five different sensors prepared at each annealing temperature are shown in Fig. 4a. All humidity sensors prepared at different annealing temperatures exhibit a linear decrease in resistance as the humidity increased from 0% to 90% RH (Fig. 4a). Furthermore, the humidity sensor processed at lower temperatures exhibits a higher response and sensitivity compared with those processed at higher temperatures, as shown in Fig. 4. For example, SDC-600 based humidity sensor exhibits approximately 20 times higher sensitivity than SDC-700, which we attribute to the higher amounts of oxygen-containing functional groups on the SDC-600 surface, as shown in Fig. 3c.

In order to investigate the conduction mechanism of the SDC film-based humidity sensor, impedance measurements were also performed, and the results are shown in Fig. S7. SDC-600 sample was deliberately chosen for AC impedance measurements because it has the highest sensitivity to humidity compared to SDC-650 and SDC-700 samples. As shown in Fig. S7a, at low frequency (<200 kHz), the humidity sensor exhibited a significant decrease in impedance with increasing humidity. However, at high frequency range, the impedance change with humidity was reduced compared to that at low frequency. This might be caused by the fact that the water molecules adsorbed on the sensor surface are difficult to align along the electrical field directions.³⁷ In addition, the Nyquist plot (Fig. S7b) exhibited a semicircular behavior without displaying Warburg impedance even at high humidity (~90% RH). From this, it is inferred that the amount of water molecule adsorbed on the surface is not enough to form a continuous layer and remains in isolated state due to relatively low hydrophilicity of the SDC film.³⁸ The relatively low hydrophilicity of the SDC film is shown in Fig. S8. Due to the p -type nature of the SDC film (Fig. S9), the water molecules form ion-dipole interaction with the carbon surface. These

adsorbed water molecules act like an oxidant and withdraw free electrons, contributing to electronic conduction of the thin carbon film.³⁹ In addition, the thin carbon film based sensor exhibited relatively low electrical resistance due to the small spacing and large facing electrode area of carbon IDEs. Thus, the electrical current flows mainly through the SDC thin film, so electronic conduction predominates. It is worth to mention that the maximum impedance response of AC measurements is comparable with the result of DC-based resistance measurement (Fig. 4a). This led to use of DC measurement technique instead of AC.

For the characterization of the response and recovery times, the SDC film-based humidity sensor was tested in a chamber, where the % RH can be rapidly varied between 0% and 70% RH. Figure 5 clearly shows that all the SDC film based humidity sensors prepared at various temperatures exhibited consistent and prompt response and recovery behaviors with negligible hysteresis during multiple cycles of humidity change; this can be attributed to its very low thickness that restricts the water kinetics mainly at the surface level, leading to fast desorption of the water molecules from the surface.⁴⁰ Specifically, the humidity sensor based on SDC-600 exhibited the fastest response of 140 ms, which increased with the annealing temperature of the SDC film. This is attributed to the difference in the amounts of sp^2 hybridization and oxygen functional groups depending on the SDC annealing temperature, as shown in Fig. 3. Reportedly, more hydroxyl groups lead to a higher affinity for water molecules¹⁶ resulting in fast response, whereas higher sp^2 carbon networks exhibit higher hydrophobicity leading to fast recovery.¹⁹ The contact angle measurements (Fig. S8) shows that the hydrophobicity of SDC film increases with the annealing temperature because the oxygen-containing functional groups decrease with the annealing temperature, as shown in Fig. 3. In addition, a longer time was required for complete recovery compared to the response due to the hydrophilicity limiting the efficient desorption of water molecules.⁴¹

To investigate the applicability of the present humidity sensor to practical environmental sensing systems, the long-term stability, power consumption, and gas interference effect were tested. For the long-term stability test, five SDC-600 based humidity sensors were prepared by the same procedure, and their response time, recovery time, and dynamic response were measured over a period of 4 weeks. As shown in Fig. 6a, their sensing characteristics remain unchanged for over 4 weeks, demonstrating the excellent stability of our SDC film based humidity sensors. Moreover, the power consumption of the SDC-600 thin film was maintained as low as ~1 mW when the sensor was operated at 1 V. Furthermore, as shown in Fig. 6b, the dynamic response of the SDC film based

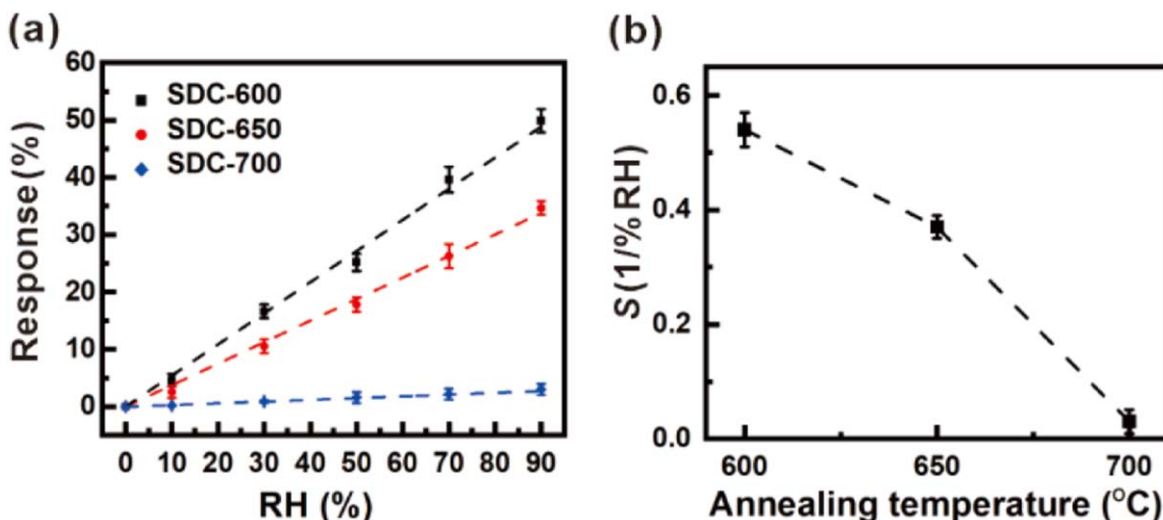


Figure 4. (a) Linear response for 0%–90% RH and (b) sensitivity of SDC film based humidity sensors prepared at various annealing temperatures (600 °C, 650 °C, and 700 °C).

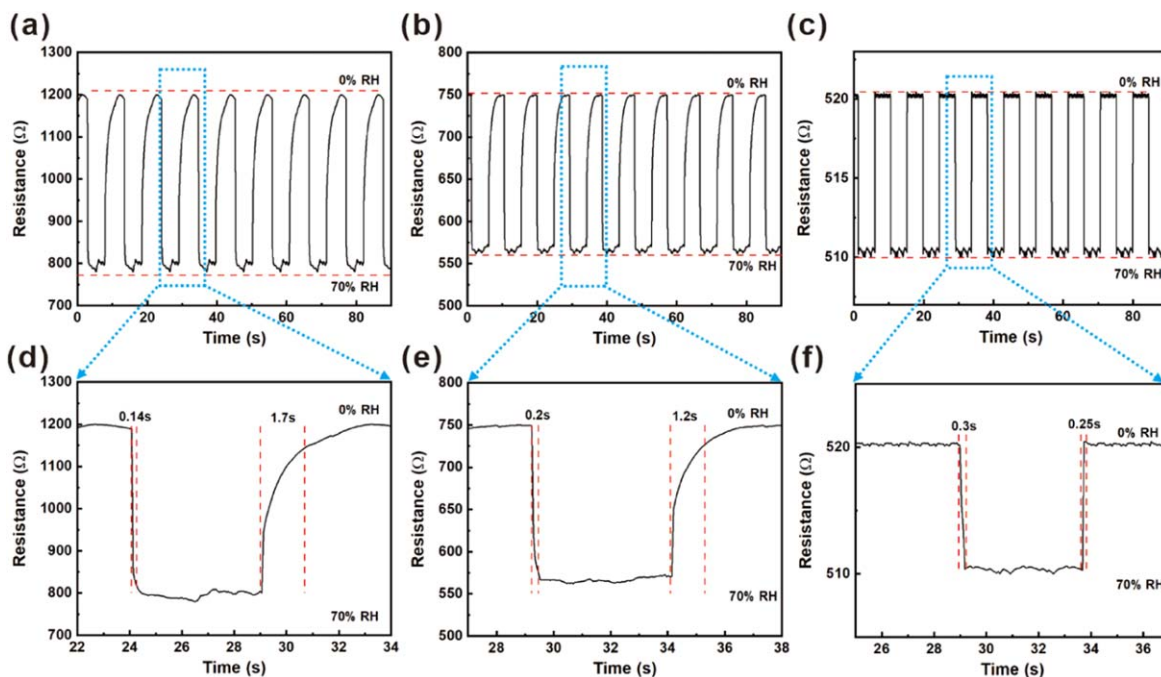


Figure 5. Response curves for repeated cycles of humidity change between 0 and 70% RH measured using humidity sensors based on (a), (d) SDC-600, (b), (e) SDC-650, and (c), (f) SDC-700.

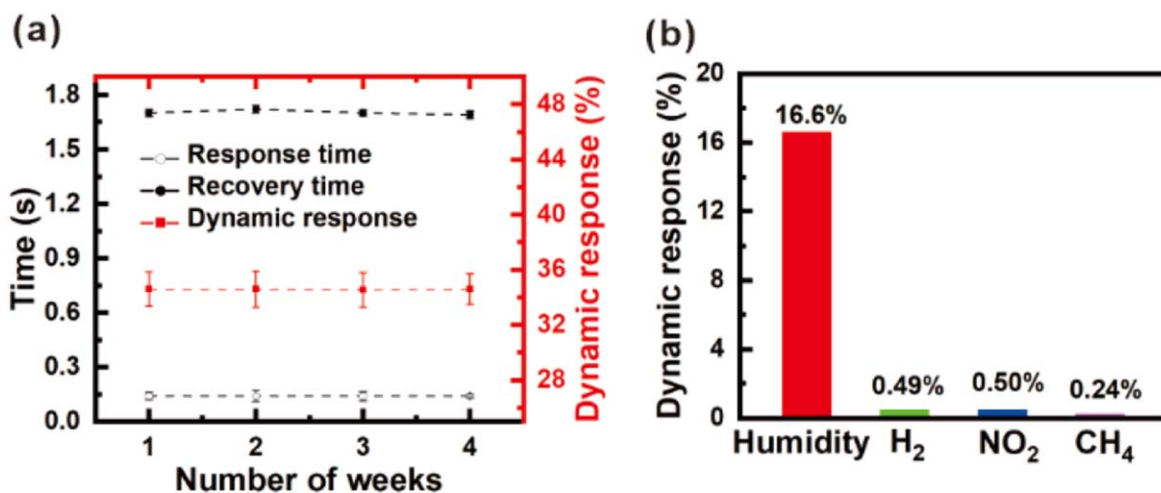


Figure 6. Long-term stability and selectivity of the SDC-600 film based humidity sensor: (a) long-term stability test results in terms of dynamic response and response/recovery times for 70% RH, (b) comparison of dynamic responses of 30% RH with various gases (1000 ppm H_2 , 5 ppm NO_2 , 1000 ppm CH_4).

humidity sensor to various gases at high concentrations (H_2 , NO_2 , and CH_4) was found to be negligible, which demonstrates its potential for accurate and reliable humidity data collection without any interference of the gas.

Table I compares the SDC thin film based humidity sensor with previously reported humidity sensors based on various active sensing materials. Compared with the previously reported metal-oxide,^{40,42} silicon carbide,⁴³ CVD grown graphene^{44,45} and rGO-based humidity sensors,^{46–48} our humidity sensors exhibit a larger dynamic response ($\sim 50\%$) along with faster response to humidity. Stefano Borini et al. reported a GO-based humidity sensor with ultrafast response in humidity-dependent impedance measurement.¹⁷ However, its narrow working humidity range (20%–70% RH) and low stability limited its practical application. Moreover, although the response of GO-based resistive humidity sensors could be significantly enhanced by doping with metal, they exhibited relatively lower sensitivity and slower response and

recovery compared with the present sensor.⁴⁹ While compromising the dynamic response, our SDC thin film based humidity sensors exhibited linear response in a wide humidity range (0%–90% RH) with excellent stability. Moreover, owing to their fast response/recovery times, excellent long-term stability, and superior selectivity, the proposed SDC thin film based humidity sensors have potential applications in the accurate and prompt calibration of gas sensors under a wide humidity range.

Conclusions

In this study, we developed a highly responsive and stable humidity sensor based on biopolymer-derived carbon thin film on sub-micrometer-sized carbon IDEs. This monolithic carbon structure was fabricated using simple thermal processes and exhibited excellent thermal compatibility and electrical connection between the thin film and cIDEs. The single-step thermal process facilitated an excellent conformal coating of the SDC thin film with strong

Table I. Comparison of SDC-600 based humidity sensors with previously reported nanomaterial-based humidity sensors.

Material	Humidity Range (% RH)	Response/Recovery Time (s)	Dynamic Response (%) ^{b)}	Sensitivity (/%RH)	Stability	References
TiO ₂ -PSS composite	30–90	2/80	N/A	N/A	4 weeks	40
VO ₂ nanoparticles	10–90	5/13	20 ^{a)}	0.25 ^{a)}	5 weeks	42
SiC nanowires	15–90	85/105	N/A	0.38 ^{a)}	6 months	43
Multilayer Graphene (CVD)	1–96	0.6/0.4	4.5	0.31 ^{a)}	N/A	44
2-Layer Graphene (CVD)	20–100	0.7/0.3	1.1	0.93 ^{a)}	N/A	45
rGO	10–70	16/47	17.6	0.02 ^{a)}	3 weeks	46
N-doped rGO	6–100	N/A	5	0.32	30 cycles	47
rGO/PU	10–70	3.5/7	9	0.53	2 weeks	48
GO (Hummer's)	20–70	0.032/0.032	N/A	N/A	72 h	17
Li-Doped GO	11–97	4/25	97	0.25 ^{a)}	N/A	49
SDC (This study)	0–90	0.14/1.7	50	0.54	4 weeks	This work

a) Estimated from graphical plot. b) Dynamic response was estimated at highest humidity condition.

adhesion on a large scale without noticeable grain boundaries or defects, leading to excellent structural stability even under high humidity conditions. The annealing temperature was found to control the crystallinity and the amount of surface functional groups of the SDC film, thereby providing an efficient means to control the sensor characteristics such as sensitivity and response/recovery times. The presented sensor demonstrated the capability of room-temperature operation and exhibited an excellent linear response with a wide humidity range. Furthermore, the sensor exhibited quick response to humidity changes owing to the large amount of oxygen-functional moieties and very small thickness of the SDC film. Furthermore, these outstanding characteristics were found to remain unchanged over four weeks. Thus, together with its long-term stability, our sensor exhibited very low power consumption, process compatibility with C-MEMS, and exceptional selectivity from various gases, which demonstrates its potential applications for IoT as well as in gas sensor calibration tools.

Acknowledgments

This research was supported by Institute of Information & Communications Technology Planning & Evaluation (IITP) grant (No. 2018-0-00756), 2019 R&D support project based on science and technology according to the regional demand (CN20120US001) funded by the Ministry of Science and ICT (MSIT, Korea), and Basic Science Research Program through the National Research Foundation of Korea(NRF) funded by the Ministry of Education (2020R1A6A1A03040570, 2016R1D1A1B03931376). We are grateful for the technical assistance received from the staff members at UCRF (UNIST Central Research Facilities) in UNIST. We would like to thank Prof. Taesung Kim and Mr. Sangjin Seo for helping in humidity sensing, Prof. Hoon-Eui Jeong and Mr. Minhoo Seong for spray-coating of shellac.

ORCID

Heungjoo Shin  <https://orcid.org/0000-0002-5660-7093>

References

- C.-Y. Lee and G.-B. Lee, *Sens. Lett.*, **3**, 1 (2005).
- A. D. Smith, Q. Li, A. Anderson, A. Vyas, V. Kuzmenko, M. Haque, L. G. H. Staaf, R. Lundgren, and P. Enoksson, *J. Phys. Conf. Ser.*, **1052**, 012143 (2018).
- J. G. D. Hester, J. Kimionis, and M. M. Tentzeris, *IEEE Trans. Microw. Theory Tech.*, **65**, 1819 (2017).
- S. S. Balpande, R. S. Pande, and R. M. Patrikar, *Sens. Actuator A-Phys.*, **251**, 134 (2016).
- M. M. Rahman, S. B. Khan, and A. M. Asiri, *PLoS One*, **9**, e85036 (2014).
- G. Korotcenkov, *Mater. Sci. Eng. R Rep.*, **61**, 1 (2008).
- J. Wu et al., *Adv. Sci.*, **4**, 1600319 (2017).
- A. Falco, F. C. Loghin, M. Becherer, P. Lugli, J. F. Salmerón, and A. Rivadeneyra, *ACS Sens.*, **4**, 3141 (2019).
- M. Masikini, M. Chowdhury, and O. Nemraoui, *J. Electrochem. Soc.*, **167**, 037537 (2020).
- Q. Ren, Y.-Q. Cao, D. Arulraj, C. Liu, D. Wu, W.-M. Li, and A.-D. Li, *J. Electrochem. Soc.*, **167**, 067528 (2020).
- K. Suematsu, K. Watanabe, M. Yuasa, T. Kida, and K. Shimanoe, *J. Electrochem. Soc.*, **166**, B618 (2019).
- S. R. Gottam, C.-T. Tsai, C.-Y. Li, and S.-Y. Chu, *J. Electrochem. Soc.*, **167**, 087507 (2020).
- I. Cho, Y. C. Sim, M. Cho, Y.-H. Cho, and I. Park, *ACS Sens.*, **5**, 563 (2020).
- E. Espid and F. Taghipour, *Sens. Actuator B-Chem.*, **241**, 828 (2017).
- C. Lv, C. Hu, J. Luo, S. Liu, Y. Qiao, Z. Zhang, J. Song, Y. Shi, J. Cai, and A. Watanabe, *Nanomaterials*, **9**, 422 (2019).
- L. Guo et al., *Carbon*, **50**, 1667 (2012).
- S. Borini, R. White, D. Wei, M. Astley, S. Haque, E. Spigone, N. Harris, J. Kivioja, and T. Ryhänen, *ACS Nano*, **7**, 11166 (2013).
- H. Bi, K. Yin, X. Xie, J. Ji, S. Wan, L. Sun, M. Terrones, and M. S. Dresselhaus, *Sci. Rep.*, **3**, 2714 (2013).
- D.-T. Phan and G.-S. Chung, *Sens. Actuator B-Chem.*, **220**, 1050 (2015).
- M. Donarelli, S. Prezioso, F. Perrozzi, L. Giancaterini, C. Cantalini, E. Treossi, V. Palermo, S. Santucci, and L. Ottaviano, *2D Mater.*, **2**, 035018 (2015).
- K. Karuppasamy, K. Prasanna, P. R. Ilango, D. Vikraman, R. Bose, A. Alfantazi, and H.-S. Kim, *J. Ind. Eng. Chem.*, **80**, 258 (2019).
- H. Lu and X. S. Zhao, *Sustain. Energ. Fuels*, **1**, 1265 (2017).
- B. Pramanick, L. B. Cadenas, D.-M. Kim, W. Lee, Y.-B. Shim, S. O. Martinez-Chapa, M. J. Madou, and H. Hwang, *Carbon*, **107**, 872 (2016).
- S.-J. Byun, H. Lim, G.-Y. Shin, T.-H. Han, S. H. Oh, J.-H. Ahn, H. C. Choi, and T.-W. Lee, *J. Phys. Chem. Lett.*, **2**, 493 (2011).
- S. R. Joshi, A. Sharma, G.-H. Kim, and J. Jang, *Mater. Sci. Eng. C*, **108**, 110465 (2020).
- J. Lee, D. Sharma, Y. Lim, and H. Shin, *Sens. Actuator B-Chem.*, **267**, 467 (2018).
- D. Sharma, J. Lee, and H. Shin, *Biosens. Bioelectron.*, **107**, 10 (2018).
- R. R. Kamath and M. J. Madou, *Anal. Chem.*, **86**, 2963 (2014).
- J. Hong, B. Kim, and H. Shin, *Nanoscale*, **10**, 14421 (2018).
- S. Sharma, A. Sharma, Y.-K. Cho, and M. Madou, *ACS Appl. Mater. Interfaces*, **4**, 34 (2012).
- S. Jiang, T. Shi, Y. Gao, H. Long, S. Xi, and Z. Tang, *J. Micromech. Microeng.*, **24**, 045001 (2014).
- E. J. H. Lee, K. Balasubramanian, R. T. Weitz, M. Burghard, and K. Kern, *Nat. Nanotechnol.*, **3**, 486 (2008).
- D. W. Yue, C. H. Ra, X. C. Liu, D. Y. Lee, and W. J. Yoo, *Nanoscale*, **7**, 825 (2015).
- Y. Lim, J.-I. Heo, M. Madou, and H. Shin, *Nanoscale Res. Lett.*, **8**, 492 (2013).
- Y. Lim, J. H. Chu, D. H. Lee, S.-Y. Kwon, and H. Shin, *J. Alloys Compd.*, **702**, 465 (2017).
- D. Yang et al., *Carbon*, **47**, 145 (2009).
- D. Zhang, X. Zong, Z. Wu, and Y. Zhang, *Sens. Actuator B-Chem.*, **266**, 52 (2018).
- W. Xie et al., *Sens. Actuator B-Chem.*, **215**, 125 (2015).
- P.-G. Su and C.-F. Chiou, *Sens. Actuator B-Chem.*, **200**, 9 (2014).
- A. Sun, L. Huang, and Y. Li, *Sens. Actuator B-Chem.*, **139**, 543 (2009).
- Z. Duan, Y. Jiang, M. Yan, S. Wang, Z. Yuan, Q. Zhao, P. Sun, G. Xie, X. Du, and H. Tai, *ACS App. Mater. Interfaces*, **11**, 21840 (2019).
- H. Yin, J. Ni, W. Jiang, Z. Zhang, and K. Yu, *Phys. E*, **43**, 1720 (2011).
- H. Y. Wang, Y. Q. Wang, Q. F. Hu, and X. J. Li, *Sens. Actuator B-Chem.*, **166–167**, 451 (2012).
- V. I. Popov, D. V. Nikolaev, V. B. Timofeev, S. A. Smagulova, and I. V. Antonova, *Nanotechnology*, **28**, 355501 (2017).
- X. Fan, K. Elgammal, A. D. Smith, M. Östling, A. Delin, M. C. Lemme, and F. Niklaus, *Carbon*, **127**, 576 (2018).
- K. Rathi and K. Pal, *ACS Omega*, **2**, 842 (2017).
- D. Zaharie-Butucel, L. Digianantonio, C. Leordean, L. Ressler, S. Astilean, and C. Farcau, *Carbon*, **113**, 361 (2017).
- S.-J. Choi, H. Yu, J.-S. Jang, M.-H. Kim, S.-J. Kim, H. S. Jeong, and I.-D. Kim, *Small*, **14**, 1703934 (2018).
- T. Q. Trung, L. T. Duy, S. Ramasundaram, and N.-E. Lee, *Nano Res.*, **10**, 2021 (2017).